

LoD-Loc v2: Aerial Visual Localization over Low Level-of-Detail City Models using Explicit Silhouette Alignment

Juelin Zhu¹, Shuaibang Peng¹, Long Wang², Hanlin Tan¹, Yu Liu¹, Maojun Zhang^{1*}, Shen Yan¹
¹National University of Defense Technology, ²Westlake University

{zhujuelin,psb24,hanlin-tan,jasonyuliu,mjzhang,yanshen12}@nudt.edu.cn, wanglongzju@gmail.com

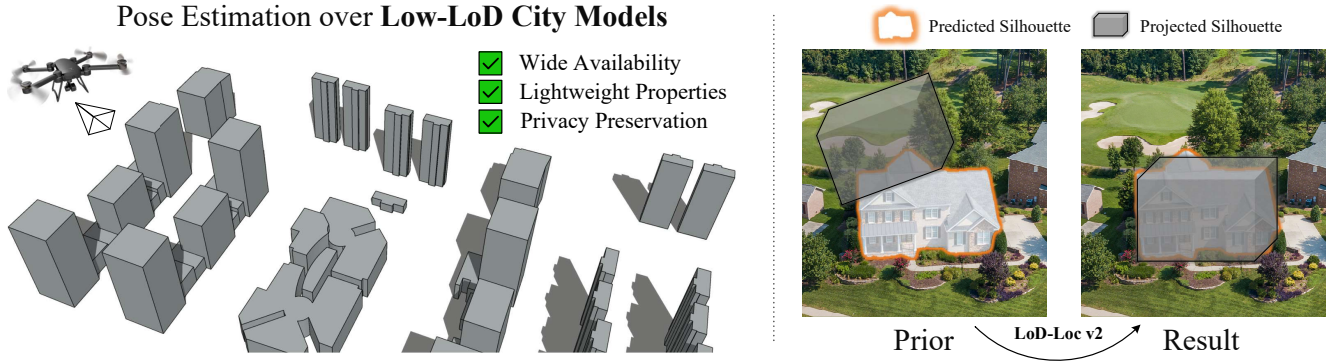


Figure 1. In this paper, we introduce LoD-Loc v2 to tackle aerial visual localization using **low-LoD** city models. These models are characterized by wide availability, lightweight properties, and inherent privacy-preserving capabilities. Given a query image with its prior pose, our approach utilizes the explicit silhouette alignment to recover the camera pose.

Abstract

We propose a novel method for aerial visual localization over **low** Level-of-Detail (LoD) city models. Previous wireframe-alignment-based method LoD-Loc [97] has shown promising localization results leveraging LoD models. However, LoD-Loc mainly relies on high-LoD (LoD3 or LoD2) city models, but the majority of available models and those many countries plan to construct nationwide are low-LoD (LoD1). Consequently, enabling localization on low-LoD city models could unlock drones’ potential for **global** urban localization. To address these issues, we introduce LoD-Loc v2, which employs a coarse-to-fine strategy using explicit silhouette alignment to achieve accurate localization over low-LoD city models in the air. Specifically, given a query image, LoD-Loc v2 first applies a building segmentation network to shape building silhouettes. Then, in the coarse pose selection stage, we construct a pose cost volume by uniformly sampling pose hypotheses around a prior pose to represent the pose probability distribution. Each cost of the volume measures the degree of alignment between the projected and predicted silhouettes. We select the pose with maximum value as the coarse pose. In the

fine pose estimation stage, a particle filtering method incorporating a multi-beam tracking approach is used to efficiently explore the hypothesis space and obtain the final pose estimation. To further facilitate research in this field, we release two datasets with LoD1 city models covering 10.7 km², along with real RGB queries and ground-truth pose annotations. Experimental results show that LoD-Loc v2 improves estimation accuracy with high-LoD models and enables localization with low-LoD models for the first time. Moreover, it outperforms state-of-the-art baselines by large margins, even surpassing texture-model-based methods, and broadens the convergence basin to accommodate larger prior errors. The project are available at <https://github.com/VictorZoo/LoD-Loc-v2>.

1. Introduction

Aerial visual localization is a task that relies on visual inputs to estimate an Unmanned Aerial Vehicle (UAV) camera’s position and orientation relative to a georeferenced map. This task plays a crucial role in the fields of computer vision and remote sensing, with applications in navigation [53], cargo transport [81], and surveillance [18, 86].

Traditional aerial visual localization algorithms [21, 86,

*Corresponding author

Name	LoD1	LoD2	LoD3
Project PLATEAU [71]	✓	✓	✓
City JSON [2]	✓	✓	
Netherlands [62]	✓	✓	
Swiss-TOPO [13]	✓	✓	
Open City Model [12]	✓		
Das 3D-Modell [4]	✓		
East Asia [72]	✓		
GABLE [76]	✓		

Table 1. **Available LoD models in different datasets.** LoD1 data is widely available across most regions, whereas LoD2 and LoD3 data are restricted to specific areas, underscoring the necessity to explore localization techniques using low-LoD models.

[92] typically rely on high-quality pre-constructed 3D geo-referenced data [60, 70, 86, 92], which offer rich structure and color features for accurate representation. However, this introduces challenges such as difficulties in data acquisition, large storage requirements, and privacy concerns. Recently, LoD-Loc [97] proposed an aggressive pipeline that utilizes LoD city models as reference maps to perform aerial visual localization. LoD models are 3D representations that focus solely on architectural structures [87], characterized by watertight geometry, object-level modeling, and hierarchical semantics across various LoDs, following the CityGML standard and its GML encoding [36, 45]. Utilizing LoD city models for visual localization offers two advantages: 1) **Light-weight properties:** LoD models are highly compact, with their storage footprint in a given area being about 10^4 times smaller than 3D texture models [97], which alleviates storage burdens for edge deployments. 2) **Privacy preservation:** Since LoD city models only shape the basic 3D outlines of buildings in a highly abstract form, they lead to fewer concerns regarding privacy disclosure.

However, a limitation of the LoD-Loc [97] approach is its reliance on high-level LoD city models, such as LoD2 or LoD3, which provide enriched structural information necessary for its proposed neural wireframe alignment method. Actually, in practical applications, the majority of available and open-source LoD models are of low detail (typically LoD1) [87], as summarized in Tab. 1. Notably, several countries, including the United States [12], China [11, 76], Switzerland [10, 13], Japan [5], Netherlands [1, 6], Singapore [8, 9] and Germany [4], have either invested in or are planning the development of nationwide LoD1 city models. Consequently, advancing research into visual localization methods that utilize low-LoD city models is pivotal for enhancing the **global** city localization capabilities of UAVs.

This task is quite challenging, as shown in Fig. 2, LoD1 models not only lack textured features but also lose significant structural details compared to high-LoD models. In

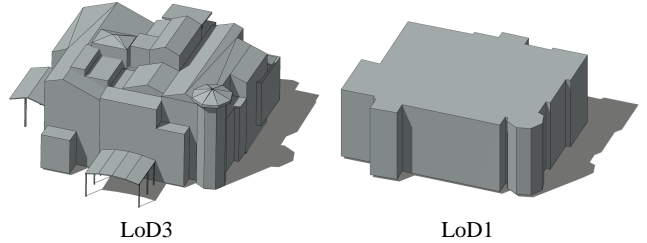


Figure 2. **Comparison between LoD3 and LoD1.** The LoD3 model provides a highly accurate representation of the building’s geometry. The LoD1 model focuses on the building’s basic shape without intricate details. Consequently, achieving effective visual localization using low-LoD city models poses a significant challenge. More details can be found in the Appendix.

this work, we explore a straightforward yet effective idea: even when wireframe representations derived from LoD1 models can not achieve precise alignment, the silhouettes remain amenable to accurate matching when the pose is correctly estimated as shown in Fig. 1. Building on this insight, we introduce LoD-Loc v2, a novel approach tailored for visual localization using low-LoD city models. Specifically, we first extract the predicted silhouettes of the query image using a segmentation network and then propose a two-stage method to gradually refine the alignment between the predicted and projected silhouettes. Given the real built-in sensor prior pose data, the coarse pose selection stage fixes the 2-DoF orientation (yaw and pitch) and generates pose hypotheses uniformly in the 3 degrees of freedom (DoF) translation and the yaw direction. Based on the generated pose hypotheses, real-time rendering technique is applied to project the LoD model onto a 2D plane, yielding the projected building silhouettes. We then score each pose hypothesis by the alignment between the projected and predicted silhouettes, thereby forming a 4D pose cost volume. The hypothesis with the highest score from the volume is selected as the coarse pose. To further enhance pose accuracy, the fine pose estimation stage employs a particle filter-based optimizer [47, 78] that iteratively explores a range of candidate hypotheses within the solution space, leading to the accurate pose recovery.

To facilitate research in this field, we release two new datasets equipped with LoD1 city models from distinct regions. Both datasets comprise drone-captured query images with priors and accurate pose annotations, spanning a total area of 10.7 km². We conduct comprehensive experiments on both the LoD1 dataset and the combined LoD2/LoD3 datasets [97]. The results demonstrate that our proposed method enables UAV localization using low-LoD city models, outperforming the LoD-Loc [97] method by a large margin and even surpassing the current state-of-the-art (SOTA) approach based on texture models [61, 80, 86]. Simultaneously, our method expands the convergence basin

to handle larger prior errors, making it a potential solution for scenarios with GPS-constrained situations.

In summary, our main contributions include:

1. We introduce a novel explicit-silhouette-alignment based framework, LoD-Loc v2, enabling aerial visual localization with low-LoD city models for the first time.
2. We release two geo-tagged LoD1 datasets covering 10.7 km², designed to facilitate future research.
3. Extensive experiments demonstrate that LoD-Loc v2 achieves outstanding localization performance in both low and high-LoD models, while also expanding the convergence basin to accommodate larger prior errors.

2. Related Works

Localization over information-rich 3D map. Conventionally, most existing methods [60, 66, 67, 75, 86] tackle pose estimation by establishing correspondences between the query image and sparse SfM [70] or mesh [60] reconstruction of the scene. The visual localization process utilizing the above 3D references can be summarized as follows: given a query image, image retrieval techniques [15, 35] are first employed to identify reference images that share similar viewpoints. Next, feature matching algorithms [29, 40, 51, 67, 75] establish accurate 2D correspondences between the query image and the identified reference images, converting these correspondences into 3D relationships by incorporating depth information. Finally, pose estimation is conducted using the PnP-RANSAC algorithm [16, 25, 26, 32, 37, 44, 93]. Despite the impressive capabilities of these 3D models in enhancing localization accuracy, they are difficult to reconstruct and maintain. Moreover, their substantial size requires considerable storage and computational resources, while their detailed information raises privacy and data protection concerns.

Localization over 2D map. In addressing the issue of map reconstruction and maintenance, some works introduce taking satellite images as references [20, 27, 73, 74, 88, 96]. The workflow of these methods generally involves constructing a georeferenced image database, dividing the target area into uniform tiles, retrieval by global descriptors [14, 15, 34], re-ranking to select the best matches [17, 38, 52, 98], and projection calculation to estimate the precise location of the query image [58]. In the context of privacy, some methods are introduced to utilizing OpenStreetMap [68, 84] or implicit neural map[69] as a reference. However, due to the lack of altitude information, these methods can estimate at most a 3-DoF pose, including planar position and heading.

Localization over LoD city model. Recently, LoD-Loc [97] proposes to leverage LoD models as the cue, which aligns LoD models projected line segments with wireframes predicted by neural networks to achieve precise pose estimation. The primary advantage of the LoD-Loc method lies

in its independence from complex 3D representations, enabling efficient and accurate visual localization using LoD models. However, the LoD-Loc method advocates localization on high-detail models at LoD3 or LoD2, which are limited in availability, thus restricting its scalability for global applications. Besides, since most of open-source LoD models are at low-LoD, it is essential to develop aerial visual localization algorithms based on low-detail models. Therefore, this paper proposes a novel visual localization method, aiming to enhance the generality and practicality of localization systems by using widely available low-LoD models.

Image segmentation. Segment Anything Model (SAM) [43] introduces a prompt-based image segmentation task aimed at outputting effective segmentation masks given input prompts, such as bounding boxes or points indicating areas of interest. As segmentation models have evolved, HQ-SAM [41] has improved the segmentation quality of the SAM model by incorporating high-quality output tokens and a global-local feature fusion strategy. Additionally, FastSAM [95], MobileSAM [94], and EfficientSAM [91] have enhanced the convenience and efficiency of the SAM model for real-time applications by optimizing the model architecture and computational efficiency. Furthermore, SAM2 [64] has strengthened the adaptability of model to dynamic environments by integrating a streaming memory architecture and multi-sensor data fusion techniques, thereby facilitating broader applications in various fields, including medical imaging [28, 55, 57, 85], motion segmentation [89], camouflage target detection [77], and building extraction [19, 65]. Inspired by these advancements, our approach first extracts building silhouettes using a segmentation network and then refines the pose to align the extracted silhouettes with the projected building silhouettes.

3. Method

Problem formulation. In typical localization tasks, the goal is to estimate the absolute 6-DoF pose of an image in the real world. In the UAV system, due to the gravity direction is provided by the onboard inertial sensors [33, 54, 68, 69, 93], the problem can be simplified to estimating a 4-DoF pose $\xi^* = (x, y, z, \theta)$, where $(x, y, z) \in \mathbb{R}^3$ denotes the translation and $\theta \in [0, 2\pi)$ is the yaw angle.

Overview - Fig. 3. Given a LoD model \mathcal{M} , a query image I_q and its prior pose estimate ξ_p , the proposed LoD-Loc v2 aims to determine the precise absolute pose ξ^* .

3.1. Building Silhouette Segmentation

We develop a SAM2-based U-like network [90] to extract building silhouettes M_q from the I_q . The network consists of SAM2 encoders, U-Net decoders, receptive field blocks (RFBs), and adapters for efficient fine-tuning [50]. Specifically, given an input query image $I_q \in \mathbb{R}^{3 \times H \times W}$, the encoder block outputs four levels of fea-

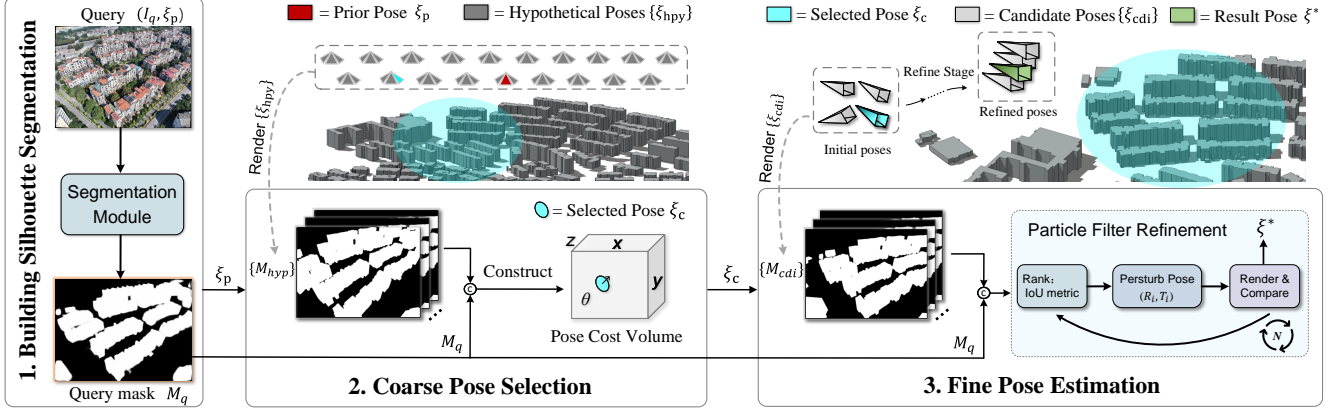


Figure 3. **Overview of LoD-Loc v2.** 1. LoD-Loc v2 employs a building segmentation module to extract building silhouettes M_q from the query image I_q (Sec. 3.1). 2. A 4D pose cost volume \mathcal{C} is built for pose hypotheses $\{\xi_{hyp}\}$ sampled around the prior pose ξ_p to select the pose ξ_c with the highest probability, based on the alignment between projected and predicted building silhouettes (Sec. 3.2). 3. A particle filter refinement is applied to refine the pose ξ_c to obtain a final accurate pose ξ^* (Sec. 3.3).

tures $F_i^e \in \mathbb{R}^{C_i \times \frac{H}{2^{i+1}} \times \frac{W}{2^{i+1}}}$ for $i \in \{1, 2, 3, 4\}$, where $C_i \in \{144, 288, 576, 1152\}$. For each F_i^e , the RFB reduces the channel count to 64, thereby yielding in $F_i^{rbf} \in \mathbb{R}^{64 \times \frac{H}{2^{i+1}} \times \frac{W}{2^{i+1}}}$ for $i \in \{1, 2, 3, 4\}$. Subsequently, the decoder blocks in the U-like structure perform sequential up-sampling, incorporating each feature layer F_i^{rbf} . The output features of each decoder block then pass through a 1×1 convolutional segmentation head, producing a corresponding segmentation result S_i for $i \in \{1, 2, 3\}$. Finally, we apply a sigmoid activation and normalization to S_1 , then threshold it at δ_s to produce the final query mask M_q . The detailed model architecture can be found in the Appendix.

3.2. Coarse Pose Selection

We sample pose hypotheses $\{\xi_{hyp}\}$ around the sensor prior pose ξ_p to construct a pose cost volume \mathcal{C} by evaluating the alignment between the projected silhouettes $\{M_{hyp}\}$ and predicted silhouettes M_q . The pose ξ_c with the highest probability in the cost volume is then selected for the next fine pose estimation stage.

Specifically, we first decouple the prior sensor pose ξ_p into six degrees, known as $(x_p, y_p, z_p, \theta_p, \rho_p, r_p)$, where (x_p, y_p, z_p) denote the translation in 3D space and (θ_p, ρ_p, r_p) represents the Euler angles, namely yaw, pitch, roll. Since the errors in the gravity direction of device sensors are negligible, we then fix the rotation axis $(\rho_c, r_c = \rho_p, r_p)$ and solely focus on the remaining 4-DoF (i.e., (x, y, z, θ)) to construct the pose cost volume \mathcal{C} . Next, we uniformly sample within the 4-DoF space centered at the prior pose ξ_p , with a sampling range of $\{r(d)\}$ and a sampling count of $\{n(d)\}$. The sampled poses $\{\xi_{hyp}\}$ are generated as:

$$\{\xi_{hyp}(d)\} = \{d_p - r(d)/2 + k \cdot \Delta s\} \quad (1)$$

where $d \in (x, y, z, \theta)$ means one of the axes, $k = \{0, 1, \dots, n(d) - 1\}$ is the index for each offset from the starting position, and $\Delta s = \frac{r(d)}{n(d)-1}$ represents the stride.

Based on each hypothetical pose ξ_{hyp} , we utilize real-time rendering technology OpenSceneGraph (OSG) [7] to project the LoD model onto a 2D plane, generating a synthetic silhouette image I_{hyp} . Subsequently, a threshold of δ_I is applied to $\{I_{hyp}\}$ to produce binary masks $\{M_{hyp}\}$. We define a silhouette alignment cost for a query image I_q across each hypothetical pose as:

$$c(I_q, I_{hyp}) = \frac{|M_q \cap M_{hyp}|}{|M_q \cup M_{hyp}|} \quad (2)$$

where $M_q \cap M_{hyp}$ means the intersection region of the predicted and projected mask, $M_q \cup M_{hyp}$ is the union region of the predicted and projected mask, and $|\cdot|$ indicates the number of pixels in the set.

By combining all hypothetical costs in a grid manner across the four dimensions (x, y, z, θ) , we obtain a pose cost volume $\mathcal{C}(I_q, I_{hyp}) = \{c(I_q, I_{hyp}^i) \mid i \in n(d)\}$. Finally, we use an *argmax* operation upon \mathcal{C} to select the coarse pose ξ_c with maximum value.

3.3. Fine Pose Estimation

To further refine the coarse pose ξ_c , inspired by [39, 40, 42, 49, 56, 63, 80], we adopt a particle filtering approach in the refinement stage to estimate the system state based on observations and dynamic adjustments.

Preliminary. The basic concept of particle filters is that, given an initial hypothesis, we can obtain new state hypotheses by perturbing the initial state, then evaluate the cost function and iteratively optimize the estimate. In a typical pose estimation task, the camera pose ξ is selected as the state variable. Starting from the initial state $\xi_c = (\mathbf{R}_c, \mathbf{t}_c)$,

Method		<i>in-Traj.</i>				<i>out-of-Traj.</i>			
		2m-2°	3m-3°	5m-5°	T.e./R.e.	2m-2°	3m-3°	5m-5°	T.e./R.e.
Prior		0	0	4.3	6.48/1.63	0	0	0.36	11.1/0.92
UAVD4L [86] <i>Texture model</i>	SIFT+NN	73.13	78.62	80.42	1.13/0.44	82.39	85.13	86.36	0.87/0.29
	SPP+SPG	91.71	92.02	92.14	0.79/0.29	93.43	93.70	93.80	0.74/0.19
	LoFTR	84.98	88.09	88.90	0.81/0.29	91.56	92.02	92.11	0.79/0.20
	e-LoFTR	84.47	88.21	88.96	0.96/0.35	91.06	91.93	92.02	0.86/0.22
	RoMA	93.27	93.70	93.77	0.78/0.25	95.03	95.53	95.53	0.73/0.22
CAD-Loc [61] <i>LoD model</i>	SIFT+NN	0	0	0	-	0	0	0	-
	SPP+SPG	0	0	0	-	0	0	0	-
	LoFTR	0	0	0	-	0	0	0	-
	e-LoFTR	0	0	0	-	0	0	0	-
	RoMA	0	0	0	-	0	0	0	-
MC-Loc [80] <i>LoD model</i>	DINOv2	1.20	4.10	17.40	8.29/2.58	2.40	7.40	26.10	7.02/2.29
	RoMa	0.10	0.60	3.30	10.6/8.60	0.20	0.90	3.30	16.9/3.88
LoD-Loc [97] <i>LoD model</i>	-	49.56	71.82	89.09	3.32/1.48	54.20	75.05	89.51	3.33/1.18
LoD-Loc v2 <i>LoD model</i>	no refine	2.99	7.73	27.87	6.19/0.67	11.68	29.88	51.14	4.78/0.92
	no select	93.50	98.40	99.50	0.74/0.17	90.50	94.80	96.90	0.77/0.16
	Full	93.70	98.40	99.50	0.72/0.15	97.90	99.80	100.00	0.71/0.14

Table 2. **Quantitative comparison results of different methods over UAVD4L-LoDv2 dataset.** T.e. and R.e. denote median translation error (m) and median rotation error (°), respectively,

where $\mathbf{t}_c \in \mathbb{R}^3$ represents the camera center and $\mathbf{R}_c \in \mathbb{R}^4$ is a quaternion that provides a stable rotation framework [48], it applies perturbations δ to generate a set of new candidate poses $\{\xi_{cdi}\}$. These candidate poses lie on the manifold of $\text{SO}(3) \times \text{T}(3)$, representing the combined rotation and translation spaces. They are subsequently evaluated and incrementally refined using the predefined loss function $\mathcal{L}(\cdot)$, thereby transforming the problem into the following optimization:

$$\xi^* = \underset{\{\xi_{cdi}\}_{i \in \text{SO}(3) \times \text{T}(3)}}{\text{argmin}} \mathcal{L}(\xi_{cdi} | I_q, I_{\xi_{cdi}}) \quad (3)$$

where $I_{\xi_{cdi}}$ is the rendered candidate.

Our approach. In our case, the particle filter models the posterior distribution of the coarse pose ξ_c as $p(\xi_c | \mathbf{Z}_i)$, where the particle set $\mathbf{Z}_i = \{(\xi_i^1, \pi_i^1), \dots, (\xi_i^n, \pi_i^n)\}$ consists of multiple particles and their corresponding weights π . Each particle’s weight π_i^j represents its sampling probability, estimated based on the Eq. (2) and Eq. (3), i.e., $\mathcal{L}(\xi | I_q, I_\xi) = \mathcal{C}(I_q, I_\xi)$. Since these particle states $\{\xi_i^1, \dots, \xi_i^n\}$ are defined on the $\text{SO}(3) \times \text{T}(3)$ manifold, they can be perturbed using Lie algebra [23, 24, 46]. Since errors along the pitch and roll axes are negligible, we keep these parameters fixed ($\rho^*, r^* = \rho_c, r_c$) and apply rotational perturbations only around the yaw axis within the $\text{SO}(3)$ subspace, while introducing translational perturbations along the (x, y, z) axes in $\text{T}(3)$ space. Additionally, to explore the hypothesis space efficiently, we adopt a multi-beam hy-

pothesis tracking approach [24, 80]. Each beam represents an independent optimization thread, allowing parallel optimization tasks to increase the likelihood of movement in the correct direction.

3.4. Supervision

The LoD-Loc v2 is trained in a supervised manner from pairs of query images I_q and ground-truth building masks G . We employ the loss function L_{seg} to supervise the building silhouette segmentation network. The L_{seg} consists of a Binary Cross-Entropy (BCE_w) loss and a weighted Intersection over Union (IoU_w) loss [31, 83], described as:

$$L_{\text{seg}} = \sum_{i=0}^2 (\text{BCE}_w[S_i, G] + \text{IoU}_w[S_i, G])_{\text{mean}} \quad (4)$$

Notice that, during the training phase, the SAM2 encoder is frozen to reduce the number of trainable parameters, thus lowering computational and storage costs.

4. Experiments

Extensive experiments are conducted on the LoD1 datasets, as well as on the LoD3 and LoD2 datasets [97], to validate the effectiveness of our proposed model.

Datasets. We release two new datasets, namely UAVD4L-LoDv2 and Swiss-EPFLv2. The UAVD4L-LoDv2 dataset covers a 2.5 km² area with georeferenced LoD1 models,

Method		<i>in-Place.</i>				<i>out-of-Place.</i>			
		2m-2°	3m-3°	5m-5°	T.e./R.e.	2m-2°	3m-3°	5m-5°	T.e./R.e.
Prior		0	0	0.56	17.6/3.87	0	0	1.06	17.9/3.94
UAVD4L [86] <i>Texture model</i>	SIFT+NN	15.17	23.74	35.11	2.57/1.54	32.98	54.35	71.50	2.76/1.59
	SPP+SPG	33.85	56.32	72.75	2.57/1.54	77.04	89.71	92.35	1.12/1.17
	LoFTR	26.40	46.21	62.22	3.06/1.86	68.87	81.00	84.96	1.12/1.08
	e-LoFTR	37.64	60.96	76.40	2.38/1.45	81.53	91.03	93.93	0.91/1.08
	RoMA	45.95	66.77	80.73	2.08/1.29	89.18	89.68	98.84	0.77/1.04
CAD-Loc [61] <i>LoD model</i>	<i>same*</i>	0	0	0	-	0	0	0	-
MC-Loc [80] <i>LoD model</i>	DINOv2	0.90	4.40	17.50	8.18/2.54	2.90	9.00	30.20	6.23/1.97
	RoMa	0.20	1.20	4.80	9.80/2.65	0.70	2.10	11.5	10.3/3.97
LoD-Loc [97] <i>LoD model</i>	-	36.79	50.56	69.77	2.87/1.78	14.24	31.39	59.89	8.73/2.78
LoD-Loc v2 <i>LoD model</i>	no refine	0.56	3.73	20.79	7.37/3.76	0.53	2.11	11.35	8.92/3.90
	no select	52.10	72.10	88.30	1.90/0.89	31.10	55.90	81.30	2.73/0.73
	Full	54.20	74.60	92.00	1.83/0.85	31.40	58.53	86.30	2.64/ 0.73

Table 3. **Quantitative comparison results of different methods over Swiss-EPFLv2 dataset.** The *same** indicates that the variants are identical to those in Tab. 2. T.e. and R.e. have the same meanings as those in Tab. 2.

which was automatically generated from the textured mesh model of the UAVD4L [86] by the DP modeler [3]. The Swiss-EPFLv2 provides a semi-automatically constructed LoD1 model, covering an 8.2 km² area. The queries in both datasets are derived from the UAVD4L-LoD and Swiss-EPFL datasets, respectively [97]. Besides, the experiments also utilized the UAVD4L-LoD and Swiss-EPFL datasets, which contain semi-automatically generated LoD3 and LoD2 models, respectively, along with drone-captured query images and pose annotations. Detailed information is provided in the Appendix and [97].

Baseline. We compare our proposed method with visual localization baselines from two categories: UAVD4L [86], which performs localization on texture models; CAD-Loc [61], MC-Loc [80], and LoD-Loc [97], which operate on LoD models. Both UAVD4L and CAD-Loc employ keypoint-based strategies: 1) the SIFT [51] descriptor with traditional Nearest Neighbor (NN) matching, 2) learning-based extractor SuperPoint (SPP) [29] with SuperGlue (SPG) [67], 3) detector-free matcher LoFTR [75] with its variant 4) e-LoFTR [82], and 5) dense feature matcher RoMa [30]. Additionally, MC-Loc utilizes two backbones as its feature extraction encoder: 6) a pre-trained DINOv2 [59] encoder, and 7) the RoMa [30] dense feature extractor. 8) LoD-Loc [97] is implemented with its default parameters. Further details on the implementation of the baseline experiments can be found in the Appendix.

Metrics. We follow standard localization evaluation metrics [79] and set thresholds at $(2m, 2^\circ)$, $(3m, 3^\circ)$, and $(5m, 5^\circ)$, as same as the LoD-Loc [97].

4.1. Implementation Details

During the training phase, the dataset for the segmentation module is derived from a subset of the synthetic images from the UAVD4L database [86], excluding images without buildings. To further enrich the training data, additional synthetic images are generated based on [86] rendering method, with pitch angles set to 30° or 60°. The ground truth mask labels G , are generated by projecting the LoD model [97] onto a 2D plane with paired poses. In total, 18,395 images of training data were generated. The segmentation module accepts input images of size $(1024, 1024)$. To optimize training, the learning rate is set to 0.001, and the AdamW optimizer is adopted with a weight decay of 5×10^{-4} to prevent overfitting. The number of training epochs is set to 20 to ensure sufficient learning. In this process, the SAM2 encoder’s pre-trained model is configured as `hiera.large`.

During the inference phase, the testing dataset differs in both area and viewpoints from the training sets, and it comprises 1) real images from the UAVD4L region and 2) real images from the Swiss-EPFL region. The input image size for the segmentation module remains $(1024, 1024)$, and the δ_s is set to 0.5. In the pose selection stage, the sizes of the query silhouettes and rendered candidates are set to $(301, 224)$ to capture approximate location information. The sampling interval is set to 10 meters and δ_I is defined as 127. In the fine pose estimation stage, the mask size is doubled to $(602, 448)$. We set the iteration count to $N = 40$, using 2 beams and an initial angular perturbation of 2 degrees. The translation perturbation follows a

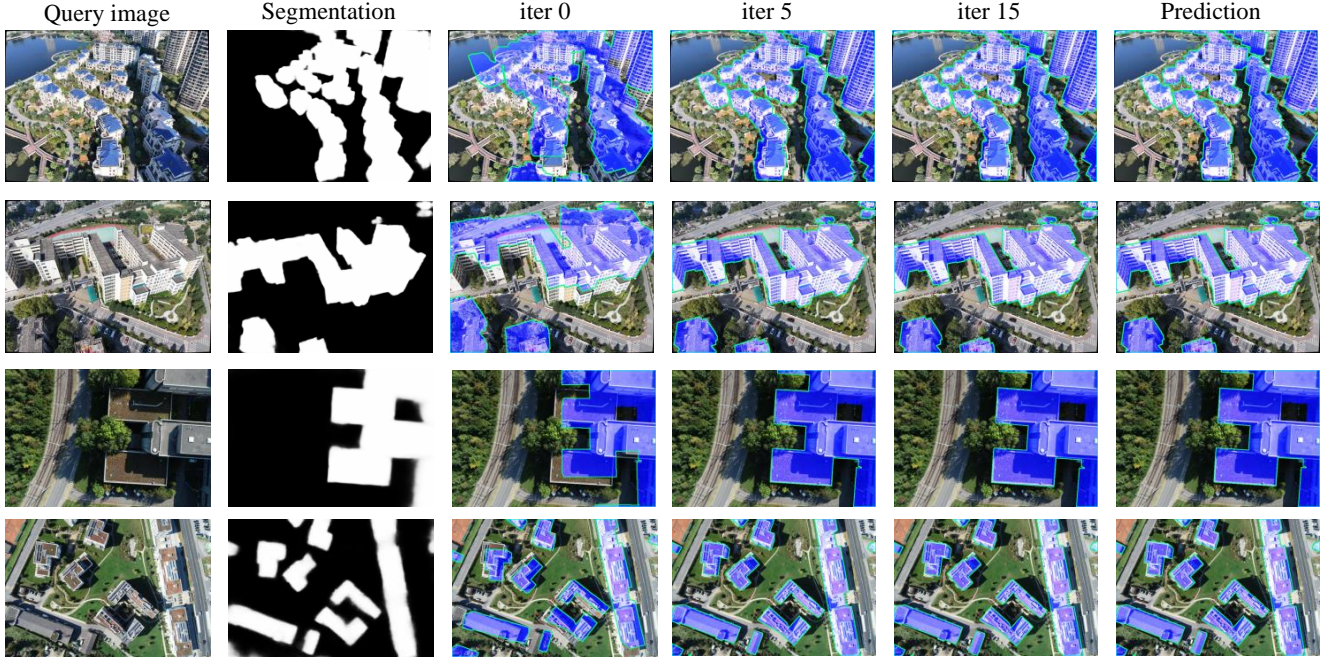


Figure 4. **Visualization of segmentation results and overlay of different iterations.** The visualized segmentation results demonstrate the model’s excellent segmentation performance. Better alignment indicates a more accurate pose prediction. Besides, the top two rows are from the UAVD4L-LoDv2 dataset, while the bottom two rows are from the Swiss-EPFLv2 dataset.

Gaussian distribution $X \sim \mathcal{N}(0, \sigma^2)$ with a mean of 0 and $\sigma = 1.5$. An attenuation coefficient $\gamma = 0.3$, and $n = 52$ candidates are generated in each iteration.

Benefiting from the OSG [7] real-time rendering technique, the rendering speed can reach $630\mu s$ at a resolution of 602×448 . The entire training and testing process was conducted on 2 NVIDIA RTX 4090 GPUs. To validate the effectiveness of our module, we experimented with three model variants: (1) -no refine, which excludes the fine pose estimation stage; (2) -no select, which skips the coarse pose selection stage; and (3) Full model represents our proposed LoD-Loc v2 model.

4.2. Evaluation Results

Evaluation over UAVD4L-LoDv2 dataset. As described in Tab. 2, our approach performs excellently in both *in-Traj.* and *out-of-Traj.* queries. While UAVD4L demonstrates impressive performance, it still encounters challenges in retrieval that result in inaccuracies in the estimated poses [97]. We further compare with CAD-Loc, MC-Loc and LoD-Loc, which leverage the same 3D reference as ours. However, CAD-Loc, and MC-Loc struggle with localization due to the large modality gap between textured and non-textured images. LoD-Loc achieves better results by leveraging line features, but the limited line information in LoD1 models directly impacts localization accuracy. Fig. 4 shows the segmentation results and visualizations of each iteration.

Model	Δ	<i>in-Traj.</i>			<i>out-of-Traj.</i>		
		(2m, 2°) / (3m, 3°) / (5m, 5°)					
LoD-Loc	30	6.86	12.9	20.9	8.12	15.4	25.6
	50	1.75	4.24	7.04	2.87	4.88	8.07
	100	0.31	1.00	1.81	1.09	1.78	2.74
	200	0.12	0.19	0.31	0.32	0.41	0.55
LoD-Loc v2	30	92.6	97.1	98.5	96.6	99.0	99.1
	50	91.3	95.1	96.7	95.9	98.3	98.5
	100	91.3	95.1	96.2	96.8	98.1	98.1
	200	90.3	94.1	95.2	94.7	97.2	97.4

Table 4. **Performance under larger prior errors.** We present results for different prior poses with added translation errors, while an analysis of orientation errors is provided in the Appendix.

Evaluation over Swiss-EPFLv2 dataset. Tab. 3 presents the inference results on the Swiss-EPFLv2 dataset. Our method is competitive for Swiss-EPFL scenes, despite being trained on UAVD4L region only. Apart from the metrics of *out-of-Place* sequence, which is lower than those in the UAVD4L [86], all other metrics surpass SOTA baselines by a large margin. Note that the comparison with texture model-based baselines is quite unfair, as these baselines use high-precision texture models enriched with detailed texture and geometry as references.

Evaluation over high-LoD dataset. We conducted exper-

Dataset	Method	<i>in-Place. (in-Traj.)</i>			<i>out-of-Place. (out-of-Traj.)</i>		
		2m-2°	3m-3°	5m-5°	2m-2°	3m-3°	5m-5°
LoD2 (Swiss-EPFL)	LoD-Loc	48.60	65.31	79.78	37.73	57.26	77.57
	LoD-Loc v2	57.90	76.00	90.60	40.40	63.90	85.80
LoD3 (UAVD4L-LoD)	LoD-Loc	84.41	91.77	96.95	95.94	99.00	99.36
	LoD-Loc v2	98.50	99.60	99.80	99.40	99.80	100.00

Table 5. **Quantitative comparison results of different methods over LoD3 and LoD2 dataset.** Compared to the LoD-Loc, our approach significantly improves visual localization performance on high-LoD models.

Method	<i>in-Traj.</i>				<i>out-of-Traj.</i>			
	2m-2°	3m-3°	5m-5°	IoU	2m-2°	3m-3°	5m-5°	IoU
FastSAM	45.3	69.8	90.1	0.39	45.6	67.2	87.4	0.31
SAM1-Ada.	86.4	94.7	98.6	0.54	96.4	97.8	98.3	0.43
Ours	93.7	98.4	99.5	0.88	97.9	99.8	100.0	0.80

Table 6. **Ablation study on different segmentation modules.** Note that each variant is fine-tuned separately, using consistent training data and input image sizes, while we keep other parameters at default settings.

iments on datasets with different levels of detail, including LoD3 (UAVD4L-LoD) and LoD2 (Swiss-EPFL), to validate the generalizability of our algorithm. Tab. 5 demonstrate that LoD-Loc v2 achieves robust and accurate localization across datasets with varying LoD levels.

4.3. Ablation Study

We conduct ablation studies on the UAVD4L-LoDv2, focusing on convergence basin and segmentation modules. More ablation studies are provided in the Appendix.

Convergence basin. We initialize different prior error ranges on the UAVD4L-LoDv2 dataset to explore the convergence basin of the proposed method. The X-Y-Z axis error ranges are set to $\Delta = \pm[30, 50, 100, 200]$ meters. As shown in Tab. 4, although the accuracy of LoD-Loc v2 decreases slightly with increasing prior error, it still outperforms LoD-Loc by a large margin. These results demonstrate that LoD-Loc v2 expands the convergence basin to accommodate larger prior errors, indicating its potential ability to solve the UAV localization problem even under GPS-constrained conditions. Fig. 5 visualizes the convergence basin with respect to translation and orientation.

Segmentation modules. As shown in Tab. 6, we used two additional segmentation models, FastSAM [95] and SAM1-Adapter [22], as backbones for our ablation studies. The results demonstrate that the U-Net segmentation module with the SAM2 encoder achieves superior performance compared to other models.

5. Conclusion

This paper introduces LoD-Loc v2, a novel method for aerial visual localization using low-LoD city models. Given

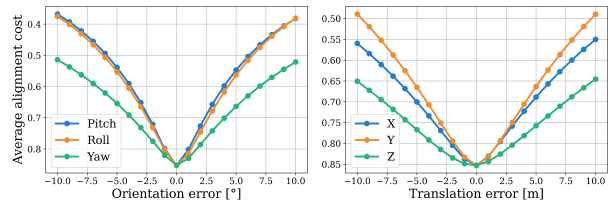


Figure 5. **Convergence basin concerning translation and orientation.** The average alignment cost is computed on the UAVD4L-LoDv2 dataset using Eq. (2).

a build-in prior pose data, LoD-Loc v2 employs a coarse-to-fine pipeline to recover the camera pose, consisting of building silhouette segmentation, coarse pose selection, and fine pose estimation. Furthermore, we contribute two novel datasets with model level of LoD1, along with real query images and ground-truth pose annotations. LoD-Loc v2 achieves excellent performance both on high-LoD and low-LoD datasets, even surpassing recent SOTA texture model-based localization techniques. Moreover, our proposed method extends the convergence basin to accommodate larger prior errors, making it a potential solution for GPS-constrained scenarios. We believe that LoD-Loc v2 opens new possibilities for global aerial visual localization by utilizing widely available low-LoD city models.

Limitation. Our method encounters limitations when building silhouettes predominantly occupying the query image. However, this situation is relatively uncommon in the context of UAV localization, where the capturing distance to buildings is typically substantial. Further analysis and visualizations are provided in the Appendix.

References

- [1] 3d bag. <https://3d.bk.tudelft.nl/projects/3dbag/>. 2
- [2] City json. <https://www.cityjson.org/datasets/>. 2
- [3] Dp modeler. <https://www.whulabs.com/DPModeler/index.aspx>. 6
- [4] Das 3d-modell. <https://www.berlin.de/sen/sbw/stadtdaten/stadtwissen/digitale-innenstadt/3d-modell/>. 2
- [5] The development and utilization of 3d city model and the introduction of disaster prevention measures in the project of data opening. https://www.bousai.go.jp/kohou/kouhoubousai/r03/102/news_05.html. 2
- [6] 3d-evolution of the dutch city of rotterdam, the netherlands. <https://geospatialworld.net/prime/case-study/aec/3d-evolution-of-the-dutch-city-of-rotterdam-the-netherlands/>. 2
- [7] Openscenegraph. <http://www.openscenegraph.com/>. 4, 7
- [8] Opening address by minister vivian balakrishnan at geo connect asia 2021, . <https://www.smartnation.gov.sg/media-hub/speeches/geo-connect-asia-2021/>. 2
- [9] Integrated environmental modeller, . <https://www.smartnation.gov.sg/initiatives/integrated-environmental-modeller/>. 2
- [10] Vision and strategic fields of action 2025. <https://www.swisstopo.admin.ch/en/vision-and-strategic-fields-of-action-2025>. 2
- [11] Ministry of natural resources fully advances the construction of real-scene 3d china. https://www.gov.cn/xinwen/2022-03/01/content_5676226.htm. 2
- [12] Open city model. <https://aws.amazon.com/marketplace/pp/prodview-q5gmfev7upw7e#resources>. 2
- [13] swissbuildings3d. <https://www.swisstopo.admin.ch/en/landscape-model-swissbuildings3d-2-0>. 2
- [14] Relja Arandjelovic and Andrew Zisserman. All about vlad. In *Proceedings of the IEEE conference on Computer Vision and Pattern Recognition*, pages 1578–1585, 2013. 3
- [15] Relja Arandjelovic, Petr Gronat, Akihiko Torii, Tomas Pajdla, and Josef Sivic. Netvlad: Cnn architecture for weakly supervised place recognition. In *Proceedings of the IEEE conference on computer vision and pattern recognition*, pages 5297–5307, 2016. 3
- [16] Daniel Barath, Jiri Matas, and Jana Noskova. Magsac: marginalizing sample consensus. In *Proceedings of the IEEE/CVF conference on computer vision and pattern recognition*, pages 10197–10205, 2019. 3
- [17] Giovanni Barbarani, Mohamad Mostafa, Hajali Bayramov, Gabriele Trivigno, Gabriele Berton, Carlo Masone, and Barbara Caputo. Are local features all you need for cross-domain visual place recognition? In *Proceedings of the IEEE/CVF Conference on Computer Vision and Pattern Recognition*, pages 6155–6165, 2023. 3
- [18] Yiming Cai, Yao Zhou, Hongwen Zhang, Yuli Xia, Peng Qiao, and Junsuo Zhao. Review of target geo-location algorithms for aerial remote sensing cameras without control points. *Applied Sciences*, 12(24):12689, 2022. 1
- [19] Keyan Chen, Chenyang Liu, Hao Chen, Haotian Zhang, Wenyuan Li, Zhengxia Zou, and Zhenwei Shi. Rsprompter: Learning to prompt for remote sensing instance segmentation based on visual foundation model. *IEEE Transactions on Geoscience and Remote Sensing*, 2024. 3
- [20] Quan Chen, Tingyu Wang, Zihao Yang, Haoran Li, Rongfeng Lu, Yaoqi Sun, Bolun Zheng, and Chenggang Yan. Sdpl: Shifting-dense partition learning for uav-view geo-localization. *IEEE Transactions on Circuits and Systems for Video Technology*, pages 1–1, 2024. 3
- [21] Shuxiao Chen, Xiangyu Wu, Mark W Mueller, and Koushil Sreenath. Real-time geo-localization using satellite imagery and topography for unmanned aerial vehicles. In *2021 IEEE/RSJ International Conference on Intelligent Robots and Systems (IROS)*, pages 2275–2281. IEEE, 2021. 1
- [22] Tianrun Chen, Lanyun Zhu, Chaotao Ding, Runlong Cao, Yan Wang, Zejian Li, Lingyun Sun, Papa Mao, and Ying Zang. Sam fails to segment anything?—sam-adapter: Adapting sam in underperformed scenes: Camouflage, shadow, medical image segmentation, and more. *arXiv preprint arXiv:2304.09148*, 2023. 8
- [23] Alessandro Chiuso and Stefano Soatto. Monte carlo filtering on lie groups. In *Proceedings of the 39th IEEE Conference on Decision and Control (Cat. No. 00CH37187)*, pages 304–309. IEEE, 2000. 5
- [24] Changyun Choi and Henrik I Christensen. Robust 3d visual tracking using particle filtering on the special euclidean group: A combined approach of keypoint and edge features. *The International Journal of Robotics Research*, 31(4):498–519, 2012. 5
- [25] Ondřej Chum and Jiří Matas. Optimal randomized ransac. *IEEE Transactions on Pattern Analysis and Machine Intelligence*, 30(8):1472–1482, 2008. 3
- [26] Ondřej Chum, Jiří Matas, and Josef Kittler. Locally optimized ransac. In *Pattern Recognition: 25th DAGM Symposium, Magdeburg, Germany, September 10-12, 2003. Proceedings 25*, pages 236–243. Springer, 2003. 3
- [27] Ming Dai, Jianhong Hu, Jiedong Zhuang, and Enhui Zheng. A transformer-based feature segmentation and region alignment method for uav-view geo-localization. *IEEE Transactions on Circuits and Systems for Video Technology*, 32(7):4376–4389, 2021. 3
- [28] Ruining Deng, Can Cui, Quan Liu, Tianyuan Yao, Lucas W Remedios, Shunxing Bao, Bennett A Landman, Lee E Wheless, Lori A Coburn, Keith T Wilson, et al. Segment anything model (sam) for digital pathology: Assess zero-shot segmentation on whole slide imaging. *arXiv preprint arXiv:2304.04155*, 2023. 3
- [29] Daniel DeTone, Tomasz Malisiewicz, and Andrew Rabinovich. Superpoint: Self-supervised interest point detection and description. In *Proceedings of the IEEE conference on*

- computer vision and pattern recognition workshops*, pages 224–236, 2018. 3, 6
- [30] Johan Edstedt, Qiyu Sun, Georg Bökman, Mårten Wadenbäck, and Michael Felsberg. Roma: Robust dense feature matching. In *Proceedings of the IEEE/CVF Conference on Computer Vision and Pattern Recognition*, pages 19790–19800, 2024. 6
- [31] Deng-Ping Fan, Ge-Peng Ji, Tao Zhou, Geng Chen, Huazhu Fu, Jianbing Shen, and Ling Shao. Pranet: Parallel reverse attention network for polyp segmentation. In *International conference on medical image computing and computer-assisted intervention*, pages 263–273. Springer, 2020. 5
- [32] Martin A Fischler and Robert C Bolles. Random sample consensus: a paradigm for model fitting with applications to image analysis and automated cartography. *Communications of the ACM*, 24(6):381–395, 1981. 3
- [33] Victor Fragoso, Joseph DeGol, and Gang Hua. gdl*: Generalized pose-and-scale estimation given scale and gravity priors. In *Proceedings of the IEEE/CVF Conference on Computer Vision and Pattern Recognition (CVPR)*, 2020. 3
- [34] Dorian Gálvez-López and Juan D Tardos. Bags of binary words for fast place recognition in image sequences. *IEEE Transactions on robotics*, 28(5):1188–1197, 2012. 3
- [35] Yixiao Ge, Haibo Wang, Feng Zhu, Rui Zhao, and Hongsheng Li. Self-supervising fine-grained region similarities for large-scale image localization. In *Computer Vision—ECCV 2020: 16th European Conference, Glasgow, UK, August 23–28, 2020, Proceedings, Part IV 16*, pages 369–386. Springer, 2020. 3
- [36] Gerhard Gröger, Thomas H Kolbe, Claus Nagel, and Karl-Heinz Häfele. Ogc city geography markup language (citygml) encoding standard. *Open Geospatial Consortium: Wayland*, 2012. 2
- [37] Bert M Haralick, Chung-Nan Lee, Karsten Ottenberg, and Michael Nölle. Review and analysis of solutions of the three point perspective pose estimation problem. *International journal of computer vision*, 13:331–356, 1994. 3
- [38] Stephen Hausler, Sourav Garg, Ming Xu, Michael Milford, and Tobias Fischer. Patch-netvlad: Multi-scale fusion of locally-global descriptors for place recognition. In *Proceedings of the IEEE/CVF conference on computer vision and pattern recognition*, pages 14141–14152, 2021. 3
- [39] Martin Humenberger, Yohann Cabon, Noé Pion, Philippe Weinzaepfel, Donghwan Lee, Nicolas Guérin, Torsten Sattler, and Gabriela Csurka. Investigating the role of image retrieval for visual localization: An exhaustive benchmark. *International Journal of Computer Vision*, 130(7):1811–1836, 2022. 4
- [40] Peter Karkus, David Hsu, and Wee Sun Lee. Particle filter networks with application to visual localization. In *Conference on robot learning*, pages 169–178. PMLR, 2018. 3, 4
- [41] Lei Ke, Mingqiao Ye, Martin Danelljan, Yu-Wing Tai, Chi-Keung Tang, Fisher Yu, et al. Segment anything in high quality. *Advances in Neural Information Processing Systems*, 36, 2024. 3
- [42] Alex Kendall, Matthew Grimes, and Roberto Cipolla. Posenet: A convolutional network for real-time 6-dof camera relocalization. In *Proceedings of the IEEE international conference on computer vision*, pages 2938–2946, 2015. 4
- [43] Alexander Kirillov, Eric Mintun, Nikhila Ravi, Hanzi Mao, Chloe Rolland, Laura Gustafson, Tete Xiao, Spencer Whitehead, Alexander C Berg, Wan-Yen Lo, et al. Segment anything. In *Proceedings of the IEEE/CVF International Conference on Computer Vision*, pages 4015–4026, 2023. 3
- [44] Laurent Kneip, Davide Scaramuzza, and Roland Siegwart. A novel parametrization of the perspective-three-point problem for a direct computation of absolute camera position and orientation. In *CVPR 2011*, pages 2969–2976. IEEE, 2011. 3
- [45] Tatjana Kutzner, Carl Smyth, Claus Nagel, Volker Coors, Diego Vinasco-Alvarez, Nobuhiro Ishimaru, Zhihang Yao, Charles Heazel, and Thomas H Kolbe. Ogc city geography markup language (citygml) version 3.0 part 2: Gml encoding standard. <https://docs.ogc.org/is/21-006r2/21-006r2.html>, 2023. 2
- [46] Junghyun Kwon and Frank C Park. Visual tracking via particle filtering on the affine group. *The International Journal of Robotics Research*, 29(2-3):198–217, 2010. 5
- [47] Junghyun Kwon, Minseok Choi, Frank Chongwoo Park, and Changmook Chun. Particle filtering on the euclidean group: framework and applications. *Robotica*, 25(6):725–737, 2007. 2
- [48] Vincent Lepetit, Pascal Fua, et al. Monocular model-based 3d tracking of rigid objects: A survey. *Foundations and Trends® in Computer Graphics and Vision*, 1(1):1–89, 2005. 5
- [49] Yunzhi Lin, Thomas Müller, Jonathan Tremblay, Bowen Wen, Stephen Tyree, Alex Evans, Patricio A Vela, and Stan Birchfield. Parallel inversion of neural radiance fields for robust pose estimation. In *2023 IEEE International Conference on Robotics and Automation (ICRA)*, pages 9377–9384. IEEE, 2023. 4
- [50] Songtao Liu, Di Huang, et al. Receptive field block net for accurate and fast object detection. In *Proceedings of the European conference on computer vision (ECCV)*, pages 385–400, 2018. 3
- [51] David G Lowe. Distinctive image features from scale-invariant keypoints. *International journal of computer vision*, 60:91–110, 2004. 3, 6
- [52] Feng Lu, Lijun Zhang, Xiangyuan Lan, Shuting Dong, Yaowei Wang, and Chun Yuan. Towards seamless adaptation of pre-trained models for visual place recognition. *arXiv preprint arXiv:2402.14505*, 2024. 3
- [53] Yuncheng Lu, Zhucun Xue, Gui-Song Xia, and Liangpei Zhang. A survey on vision-based uav navigation. *Geospatial information science*, 21(1):21–32, 2018. 1
- [54] Simon Lynen, Bernhard Zeisl, Dror Aiger, Michael Bosse, Joel Hesch, Marc Pollefeys, Roland Siegwart, and Torsten Sattler. Large-scale, real-time visual-inertial localization revisited. *The International Journal of Robotics Research*, 39(9):1061–1084, 2020. 3
- [55] Jun Ma, Yuting He, Feifei Li, Lin Han, Chenyu You, and Bo Wang. Segment anything in medical images. *Nature Communications*, 15(1):654, 2024. 3

- [56] Dominic Maggio, Marcus Abate, Jingnan Shi, Courtney Mario, and Luca Carlone. Loc-nerf: Monte carlo localization using neural radiance fields. In *2023 IEEE International Conference on Robotics and Automation (ICRA)*, pages 4018–4025. IEEE, 2023. 4
- [57] Maciej A Mazurowski, Haoyu Dong, Hanxue Gu, Jichen Yang, Nicholas Konz, and Yixin Zhang. Segment anything model for medical image analysis: an experimental study. *Medical Image Analysis*, 89:102918, 2023. 3
- [58] Ivan Moskalenko, Anastasiia Kornilova, and Gonzalo Ferrer. Visual place recognition for aerial imagery: A survey. *arXiv preprint arXiv:2406.00885*, 2024. 3
- [59] Maxime Oquab, Timothée Darcet, Théo Moutakanni, Huy Vo, Marc Szafraniec, Vasil Khalidov, Pierre Fernandez, Daniel Haziza, Francisco Massa, Alaaeldin El-Nouby, et al. Dinov2: Learning robust visual features without supervision. *arXiv preprint arXiv:2304.07193*, 2023. 6
- [60] Vojtech Panek, Zuzana Kukelova, and Torsten Sattler. Meshloc: Mesh-based visual localization. In *European Conference on Computer Vision*, pages 589–609. Springer, 2022. 2, 3
- [61] Vojtech Panek, Zuzana Kukelova, and Torsten Sattler. Visual localization using imperfect 3d models from the internet. In *Proceedings of the IEEE/CVF Conference on Computer Vision and Pattern Recognition*, pages 13175–13186, 2023. 2, 5, 6
- [62] Ravi Peters, Balázs Dukai, Stelios Vitalis, Jordi van Liempt, and Jantien Stoter. Automated 3d reconstruction of lod2 and lod1 models for all 10 million buildings of the netherlands. *Photogrammetric Engineering & Remote Sensing*, 88(3):165–170, 2022. 2
- [63] Maxime Pietrantonì, Martin Humenberger, Torsten Sattler, and Gabriela Csurka. Segloc: Learning segmentation-based representations for privacy-preserving visual localization. In *Proceedings of the IEEE/CVF Conference on Computer Vision and Pattern Recognition*, pages 15380–15391, 2023. 4
- [64] Nikhila Ravi, Valentin Gabeur, Yuan-Ting Hu, Ronghang Hu, Chaitanya Ryali, Tengyu Ma, Haitham Khedr, Roman Rädle, Chloe Rolland, Laura Gustafson, et al. Sam 2: Segment anything in images and videos. *arXiv preprint arXiv:2408.00714*, 2024. 3
- [65] Simiao Ren, Francesco Luzi, Saad Lahrichi, Kaleb Kassaw, Leslie M Collins, Kyle Bradbury, and Jordan M Malof. Segment anything, from space? In *Proceedings of the IEEE/CVF Winter Conference on Applications of Computer Vision*, pages 8355–8365, 2024. 3
- [66] Paul-Edouard Sarlin, Cesar Cadena, Roland Siegwart, and Marcin Dymczyk. From coarse to fine: Robust hierarchical localization at large scale. In *Proceedings of the IEEE/CVF conference on computer vision and pattern recognition*, pages 12716–12725, 2019. 3
- [67] Paul-Edouard Sarlin, Daniel DeTone, Tomasz Malisiewicz, and Andrew Rabinovich. Superglue: Learning feature matching with graph neural networks. In *Proceedings of the IEEE/CVF conference on computer vision and pattern recognition*, pages 4938–4947, 2020. 3, 6
- [68] Paul-Edouard Sarlin, Daniel DeTone, Tsun-Yi Yang, Armen Avetisyan, Julian Straub, Tomasz Malisiewicz, Samuel Rota Bulo, Richard Newcombe, Peter Kotschieder, and Vasileios Balntas. Orienternet: Visual localization in 2d public maps with neural matching. In *Proceedings of the IEEE/CVF Conference on Computer Vision and Pattern Recognition*, pages 21632–21642, 2023. 3
- [69] Paul-Edouard Sarlin, Eduard Trulls, Marc Pollefeys, Jan Hosang, and Simon Lymen. Snap: Self-supervised neural maps for visual positioning and semantic understanding. *Advances in Neural Information Processing Systems*, 36, 2024. 3
- [70] Johannes L Schonberger and Jan-Michael Frahm. Structure-from-motion revisited. In *Proceedings of the IEEE conference on computer vision and pattern recognition*, pages 4104–4113, 2016. 2, 3
- [71] T Seto, T Furuhashi, and Y Uchiyama. Role of 3d city model data as open digital commons: a case study of openness in japan’s digital twin” project plateau”. *The International Archives of the Photogrammetry, Remote Sensing and Spatial Information Sciences*, 48:201–208, 2023. 2
- [72] Qian Shi, Jiajun Zhu, Zhengyu Liu, Haonan Guo, Song Gao, Mengxi Liu, Zihong Liu, and Xiaoping Liu. The last puzzle of global building footprints—mapping 280 million buildings in east asia based on vhr images. *Journal of Remote Sensing*, 4:0138, 2024. 2
- [73] Yujiao Shi and Hongdong Li. Beyond cross-view image retrieval: Highly accurate vehicle localization using satellite image. In *Proceedings of the IEEE/CVF Conference on Computer Vision and Pattern Recognition*, pages 17010–17020, 2022. 3
- [74] Yujiao Shi, Xin Yu, Dylan Campbell, and Hongdong Li. Where am i looking at? joint location and orientation estimation by cross-view matching. In *Proceedings of the IEEE/CVF Conference on Computer Vision and Pattern Recognition*, pages 4064–4072, 2020. 3
- [75] Jiaming Sun, Zehong Shen, Yuang Wang, Hujun Bao, and Xiaowei Zhou. Loftr: Detector-free local feature matching with transformers. In *Proceedings of the IEEE/CVF conference on computer vision and pattern recognition*, pages 8922–8931, 2021. 3, 6
- [76] Xian Sun, Xingliang Huang, Yongqiang Mao, Taowei Sheng, Jihao Li, Zhirui Wang, Xue Lu, Xiaoliang Ma, Deke Tang, and Kaiqiang Chen. Gable: A first fine-grained 3d building model of china on a national scale from very high resolution satellite imagery. *Remote Sensing of Environment*, 305: 114057, 2024. 2
- [77] Lv Tang, Haoke Xiao, and Bo Li. Can sam segment anything? when sam meets camouflaged object detection. *arXiv preprint arXiv:2304.04709*, 2023. 3
- [78] Sebastian Thrun. Probabilistic robotics. *Communications of the ACM*, 45(3):52–57, 2002. 2
- [79] Carl Toft, Will Maddern, Akihiko Torii, Lars Hammarstrand, Erik Stenborg, Daniel Safari, Masatoshi Okutomi, Marc Pollefeys, Josef Sivic, Tomas Pajdla, et al. Long-term visual localization revisited. *IEEE Transactions on Pattern Analysis and Machine Intelligence*, 44(4):2074–2088, 2020. 6
- [80] Gabriele Trivigno, Carlo Masone, Barbara Caputo, and Torsten Sattler. The unreasonable effectiveness of pre-trained features for camera pose refinement. In *Proceedings*

- of the *IEEE/CVF Conference on Computer Vision and Pattern Recognition*, pages 12786–12798, 2024. 2, 4, 5, 6
- [81] Daniel KD Villa, Alexandre S Brandao, and Mário Sarcinelli-Filho. A survey on load transportation using multirotor uavs. *Journal of Intelligent & Robotic Systems*, 98: 267–296, 2020. 1
- [82] Yifan Wang, Xingyi He, Sida Peng, Dongli Tan, and Xiaowei Zhou. Efficient lofr: Semi-dense local feature matching with sparse-like speed. In *Proceedings of the IEEE/CVF Conference on Computer Vision and Pattern Recognition*, pages 21666–21675, 2024. 6
- [83] Jun Wei, Shuhui Wang, and Qingming Huang. F³net: fusion, feedback and focus for salient object detection. In *Proceedings of the AAAI conference on artificial intelligence*, pages 12321–12328, 2020. 5
- [84] Hang Wu, Zhenghao Zhang, Siyuan Lin, Xiangru Mu, Qiang Zhao, Ming Yang, and Tong Qin. Maplocnet: Coarse-to-fine feature registration for visual re-localization in navigation maps. *arXiv preprint arXiv:2407.08561*, 2024. 3
- [85] Junde Wu, Wei Ji, Yuanpei Liu, Huazhu Fu, Min Xu, Yanwu Xu, and Yueming Jin. Medical sam adapter: Adapting segment anything model for medical image segmentation. *arXiv preprint arXiv:2304.12620*, 2023. 3
- [86] Rouwan Wu, Xiaoya Cheng, Juelin Zhu, Yuxiang Liu, Maojun Zhang, and Shen Yan. Uavd4l: A large-scale dataset for uav 6-dof localization. In *2024 International Conference on 3D Vision (3DV)*, pages 1574–1583. IEEE, 2024. 1, 2, 3, 5, 6, 7
- [87] Olaf Wysocki, Benedikt Schwab, Christof Beil, Christoph Holst, and Thomas H Kolbe. Reviewing open data semantic 3d city models to develop novel 3d reconstruction methods. *The International Archives of the Photogrammetry, Remote Sensing and Spatial Information Sciences*, 48:493–500, 2024. 2
- [88] Zimin Xia, Olaf Booij, Marco Manfredi, and Julian FP Kooij. Visual cross-view metric localization with dense uncertainty estimates. In *European Conference on Computer Vision*, pages 90–106. Springer, 2022. 3
- [89] Junyu Xie, Charig Yang, Weidi Xie, and Andrew Zisserman. Moving object segmentation: All you need is sam (and flow). *arXiv preprint arXiv:2404.12389*, 2024. 3
- [90] Xinyu Xiong, Zihuang Wu, Shuangyi Tan, Wenxue Li, Feilong Tang, Ying Chen, Siying Li, Jie Ma, and Guanbin Li. Sam2-UNET: Segment anything 2 makes strong encoder for natural and medical image segmentation. *arXiv preprint arXiv:2408.08870*, 2024. 3
- [91] Yunyang Xiong, Bala Varadarajan, Lemeng Wu, Xiaoyu Xiang, Fanyi Xiao, Chenchen Zhu, Xiaoliang Dai, Dilin Wang, Fei Sun, Forrest Iandola, et al. EfficientSAM: Leveraged masked image pretraining for efficient segment anything. In *Proceedings of the IEEE/CVF Conference on Computer Vision and Pattern Recognition*, pages 16111–16121, 2024. 3
- [92] Shen Yan, Xiaoya Cheng, Yuxiang Liu, Juelin Zhu, Rouwan Wu, Yu Liu, and Maojun Zhang. Render-and-compare: Cross-view 6-dof localization from noisy prior. In *2023 IEEE International Conference on Multimedia and Expo (ICME)*, pages 2171–2176. IEEE, 2023. 2
- [93] Shen Yan, Yu Liu, Long Wang, Zehong Shen, Zhen Peng, Haomin Liu, Maojun Zhang, Guofeng Zhang, and Xiaowei Zhou. Long-term visual localization with mobile sensors. In *Proceedings of the IEEE/CVF Conference on Computer Vision and Pattern Recognition*, pages 17245–17255, 2023. 3
- [94] Chaoning Zhang, Dongshen Han, Yu Qiao, Jung Uk Kim, Sung-Ho Bae, Seungkyu Lee, and Choong Seon Hong. Faster segment anything: Towards lightweight sam for mobile applications. *arXiv preprint arXiv:2306.14289*, 2023. 3
- [95] Xu Zhao, Wenchao Ding, Yongqi An, Yinglong Du, Tao Yu, Min Li, Ming Tang, and Jinqiao Wang. Fast segment anything. *arXiv preprint arXiv:2306.12156*, 2023. 3, 8
- [96] Zhedong Zheng, Yunchao Wei, and Yi Yang. University-1652: A multi-view multi-source benchmark for drone-based geo-localization. In *Proceedings of the 28th ACM international conference on Multimedia*, pages 1395–1403, 2020. 3
- [97] Juelin Zhu, Shen Yan, Long Wang, zhang shengYue, Yu Liu, and Maojun Zhang. Lod-loc: Aerial visual localization using lod 3d map with neural wireframe alignment. In *Advances in Neural Information Processing Systems*, pages 119063–119098, 2024. 1, 2, 3, 5, 6, 7
- [98] Sijie Zhu, Linjie Yang, Chen Chen, Mubarak Shah, Xiaohui Shen, and Heng Wang. R2former: Unified retrieval and reranking transformer for place recognition. In *Proceedings of the IEEE/CVF Conference on Computer Vision and Pattern Recognition*, pages 19370–19380, 2023. 3